Double fermiophobic Higgs boson production at the CERN LHC and a linear collider

A. G. Akeroyd,[1] Marco A. Díaz,[2] and Francisco J. Pacheco[2]

[1]*Korea Institute for Advanced Study, 207-43 Cheongryangri 2-dong, Dongdaemun-gu, Seoul 130-722, Republic of Korea*
[2]*Departamento de Física, Universidad Católica de Chile, Avenida Vicuña Mackenna 4860, Santiago, Chile*

We consider the phenomenology of a fermiophobic Higgs boson (h_f) at the Large Hadron Collider (LHC) and a e^+e^- linear collider (LC). At both machines the standard production mechanisms which rely on the coupling $h_f VV$ ($V = W^\pm, Z$) can be very suppressed at large $\tan\beta$. In such cases the complementary channels $pp \to H^\pm h_f, A^0 h_f$ and $e^+e^- \to A^0 h_f$ offer promising cross sections. Together with the potentially large branching ratios for $H^\pm \to h_f W^*$ and $A^0 \to h_f Z^*$, these mechanisms would give rise to double h_f production, leading to signatures of $\gamma\gamma\gamma\gamma$, $\gamma\gamma VV$ and $VVVV$.

I. INTRODUCTION

Neutral Higgs bosons (h^0) with branching ratios (BRs), very different to those of the standard model (SM) Higgs boson ϕ^0, can arise in extensions of the SM which contain an additional SU(2) × U(1) Higgs doublet, the "Two Higgs Doublet Model" (2HDM) [1]. The assumption that each fermion type (up/down) couples to only one Higgs doublet [2], which eliminates tree-level Higgs mediated flavor changing neutral currents, leads to four distinct versions of the 2HDM [3]. No compelling experimental evidence has been found for Higgs bosons. Experimental searches for ϕ^0 at LEP concentrated on the channel $\phi^0 \to b\bar{b}$ [4], while more recently [5] searches for Higgs bosons with large BR to lighter fermions and gluons (i.e., $c\bar{c}$, $\tau^+\tau^-$, gg [6]) were performed. The phenomena known as "fermiophobia" , which signifies very suppressed or zero coupling to the fermions, may arise in a particular version of the 2HDM called type I [8] or in models with Higgs triplets [9]. Depending on its mass, a fermiophobic Higgs (h_f) [10–16] would decay dominantly to two photons, $h_f \to \gamma\gamma$, for $m_{h_f} < 95$ GeV or to two massive gauge bosons, $h_f \to VV^{(*)}$, ($V = W^\pm, Z$) if $m_{h_f} > 95$ GeV [12,13]. The large BR to $\gamma\gamma$ would give a very clear experimental signature, and observation of such a particle would strongly constrain the possible choices of the underlying Higgs sector.

Experimental searches for fermiophobic Higgs bosons at LEP and Fermilab have been negative so far. Lower bounds of the order $m_{h_f} \gtrsim 100$ GeV have been obtained by the LEP collaborations OPAL [17], DELPHI [18], ALEPH [19], and L3 [20], utilizing the channel $e^+e^- \to h_f Z$, $h_f \to \gamma\gamma$. Only L3 [21] has considered $h_f \to WW^*$ decays. OPAL [17] and DELPHI [18] also searched in the channel $e^+e^- \to h_f A^0$, $h_f \to \gamma\gamma$. From the Tevatron Run I, the limits on m_{h_f} from the D0 and CDF collaborations are, respectively, 78.5 GeV [22] and 82 GeV [23] at 95% C.L., using the mechanism $qq' \to V^* \to h_f V, h_f \to \gamma\gamma$, with the dominant contribution coming from $V = W^\pm$.

Run II will extend the coverage of m_{h_f} beyond that of LEP [24,25].
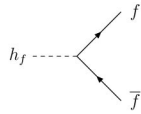
All the above mass limits, however, assume that the $h_f VV$ coupling is of the same strength as the SM coupling $\phi^0 VV$, which in general would not be the case for a h_f in a realistic model in which the $h_f VV$ coupling has an additional suppression from a mixing angle. Such a scenario would enable a very light h_f ($m_{h_f} < < 100$ GeV) to escape the searches at LEP and the Tevatron Run I. Therefore, it is of interest to consider other production mechanisms for h_f which may still allow observable rates even when the $h_f VV$ coupling is suppressed. In a previous paper [26] we proposed several new production mechanisms at the Tevatron Run II. In particular, the process $p\bar{p} \to H^\pm h_f$ offers promising rates if the masses of both $H^\pm$ and h_f are less than 100 GeV. These complementary mechanisms cover some of the region of suppressed coupling $h_f VV$, particularly if $m_{h_f} < 80$ GeV. However, for heavier m_{h_f} (> 80 GeV), detection prospects are diminished due to phase space suppression at the Tevatron energy. In this paper we extend the analysis of [26] to consider the search potential at two future colliders, the Large Hadron Collider (LHC) and a e^+e^- linear collider (LC). These colliders will offer significantly improved detection prospects for h_f, and in case of a h_f being detected in Run II would allow a more precise determination of its properties. Our work is organized as follows: In Section II we give a brief introduction to fermiophobic Higgs bosons. Section III covers the production of h_f at the LHC and LC, while Section IV contains our numerical results. Conclusions are given in Section V.

II. FERMIOPHOBIC HIGGS BOSONS

The first studies of the phenomenology of h_f can be found in [10,11]. BRs for h_f were presented in [12,13], while its phenomenology at the Tevatron Run I was covered in [12,14]. Production at LEP2 and the impact of
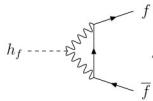
charged scalar loops on BR ($h_f \rightarrow \gamma\gamma$) (mediated via the trilinear coupling $h_f H^+ H^-$) were studied in [15,16].

Such a particle may arise in a 2HDM in which one SU(2) × U(1) Higgs doublet (Φ_2) couples to all fermion types, while the other doublet (Φ_1) does not. This model is usually called "Type I" [8]. Because of the mixing in the CP-even neutral Higgs mass matrix (which is diagonalized by α) both CP-even eigenstates h^0 and H^0 can couple to the fermions. The fermionic couplings of the lightest CP-even Higgs h^0 take the form $h^0 f\bar{f} \sim \cos\alpha/\sin\beta$, where f is any fermion and β is defined by $\tan\beta = v_2/v_1$ (where v_i is the vacuum expectation value of the ith doublet). Small values of $\cos\alpha$ would strongly suppress the fermionic couplings, and in the limit $\cos\alpha \rightarrow 0$ the coupling $h^0 f\bar{f}$ would vanish at tree level, giving rise to fermiophobia,

Exact tree-level fermiophobia is not stable under radiative corrections [13,15]. One can estimate what sort of deviation from exact fermiophobia we could expect by considering as an example the quantum correction involving two W. To estimate the order of magnitude of this correction we approximate
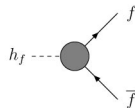

where C is a generic triangular Veltman's function. If we approximate $C \sim 1/m_h^2$, expected in the limit of large Higgs mass, and compare this correction with the tree-level vertex in the SM $g_{hff} \sim gm_f/2m_W$ we find,

$$\frac{\Delta g_{hff}}{g_{hff}} \sim \frac{g^2}{64\pi^2}\left(\frac{m_W}{m_h}\right)^2 \sim 10^{-4}, \qquad (1)$$

for a Higgs mass twice as large as the W mass. This indicates that tree-level fermiophobia is weakly affected by quantum corrections.

In general one would expect approximate fermiophobia, with some small coupling to fermions:

Of course, the correct renormalization of this vertex involves counterterms that need to be fixed with experimental measurements. We mention two examples in the literature on how this counterterm can be fixed. In the first example [16] the authors set $\cos\alpha = 0$ at tree level, *i.e.,*

tree-level fermiophobia. In this case, the one-loop contributions to the $h_f f\bar{f}$ coupling are finite and therefore the counterterm is finite as well. The finite part of the counterterm is also chosen to be zero, such that the renormalized coupling becomes equal to the sum of the finite one-loop graphs that contribute to it. In this scheme, $\cos\alpha = 0$ means tree-level fermiophobia, and at one loop the coupling $h_f f\bar{f}$ is not zero, although small, inducing a small $h_f \rightarrow b\bar{b}$ branching ratio as observed in their figures.

In the second example [27], the authors are concerned with the one-loop fermionic decay width in the context of the 2HDM (Model II), but nevertheless their results can be adapted to the case of h_f in the 2HDM (Model I). In [27] the counterterm for the angle α is chosen such that there is no mixing between h and H. This means that α is the mixing angle at one loop implying that the one-loop coupling $h_f f\bar{f}$ is proportional to $\cos\alpha$, as can be seen from their formula for the decay width to fermions. In this scheme, $\cos\alpha = 0$ means one-loop fermiophobia, and therefore the definitions for α in the two schemes are not equivalent, and a relation between the two parameters α must be derived in order to compare.

The main decay modes of a fermiophobic Higgs are $h_f \rightarrow \gamma\gamma, W^*W^*, Z^*Z^*$. Assuming that $h_f \rightarrow \gamma\gamma$ is primarily mediated by the W loop, this photonic channel is dominant for $m_{h_f} \lesssim 95$ GeV, with a BR near 100% for $m_{h_f} \lesssim 80$ GeV, decreasing to 50% at $m_{h_f} \approx 95$ GeV and to 1% at $m_{h_f} \approx 145$ GeV. In contrast, BR($\phi^0 \rightarrow \gamma\gamma) \approx 0.22\%$ is the largest value in the SM, occurring around $m_{\phi^0} = 120$ GeV. The photonic decay mode is a particularly robust sign of fermiophobia for $m_{h_f} \lesssim 150$ GeV, above which BR($h_f \rightarrow \gamma\gamma$) approaches the SM value. Fermiophobic models permit the largest BRs to two photons, but (smaller) enhancements relative to the SM BR are also possible in other models where a neutral Higgs boson (h^0) couples to some but not all quarks, either by choosing appropriate mixing angles [28] or as a consequence of model building [24,29]. Enhancements of BR($h^0 \rightarrow \gamma\gamma$) due to the scalar loop contribution were studied in [27,30] in the decoupling limit of the 2HDM (Model II). In this paper we will focus on h_f from the 2HDM (Model I).

III. h_f PRODUCTION AT LHC AND LC

In this section we consider the production of h_f at the LHC and LC, in both the standard mechanisms (which depend on the $h_f VV$ coupling), and the complementary mechanisms which produce h_f together with another Higgs boson and depend on the $h_f HV$ coupling with $H = H^\pm$ or A^0. For studies of these complementary mechanisms in the context of models without a h_f, see [31]. We will present the cross sections as a function of m_{h_f}, $\tan\beta$

and $m_{H^\pm}/m_A$. Our analysis can be applied to two different scenarios:

(i) *Detection* of a h_f at the Tevatron Run II. In this case the LHC and LC would provide confirmation as well as further studies of the h_f properties.

(ii) *Nonobservation* of a h_f at the Tevatron Run II. In this case the LHC and LC would probe a significantly larger parameter space of m_{h_f} and $\tan\beta$.

In the case of h_f production at e^+e^- colliders, the complementary mechanism has been exploited at LEP [17,18], which searched for $e^+e^- \to A^0 h_f$. So far, complementary mechanisms have not been considered at the Tevatron. As emphasized in [26], a more complete search strategy for h_f at hadron colliders would include such production processes.

A. Standard mechanisms

At the LHC there are two standard ways to produce h_f, for which experimental simulations have been performed in the context of the SM Higgs boson (ϕ^0). These are:

(i) $pp \to W^* \to W h_f$, $W \to l\nu$ (Higgsstrahlung) [32].

(ii) $pp \to qq h_f$ (Vector boson fusion) [33,34]. At an e^+e^- LC one has the following mechanisms:

(iii) $e^+e^- \to h_f Z$ (Higgsstrahlung) [35].

(iv) $e^+e^- \to h_f \nu\bar\nu$ (W boson fusion) [35].

All the above mechanisms have been shown to be effective for ϕ^0 due to its substantial coupling to vector bosons (for a recent application of the above processes to h^0 of the minimal supersymmetric standard model see [36]). This is not necessarily the case in the 2HDM, in which a h_f may arise. In the 2HDM the mechanisms (i) to (iv) for h_f are all suppressed by $\sin^2(\beta - \alpha)$, which in the tree-level fermiophobic limit ($\alpha \to \pi/2$) in Model I simplifies to:

$$VVh_f \sim \cos^2\beta[\equiv 1/(1 + \tan^2\beta)]. \qquad (2)$$

This is a severe suppression for $\tan\beta \gtrsim 10$ and renders all the above mechanisms unobservable (for an earlier discussion with just mechanism (i) see [28]). This is shown in Fig. 1 where we apply the results of the signal/background ($S^\phi/\sqrt{B}$) simulations for $\phi^0 \to \gamma\gamma$ to the case of a h_f. To do this we need to scale the SM Higgs signal S^ϕ by the factor $\mathrm{BR}(h_f \to \gamma\gamma)/\mathrm{BR}(\phi^0 \to \gamma\gamma)$, and include the $\cos^2\beta$ suppression in the production cross sections. Our aim is to merely show the strong dependence of $S/\sqrt{B}$ on $\tan\beta$. We show results for $S/\sqrt{B} > 1$ and are not concerned with additional statistical and systematic considerations associated with small signal rates. Since all the above simulations presented results for $m_{\phi^0} = 120$ GeV we will consider a h_f of this mass. For $m_{h_f} = 120$ GeV one has [12,13]
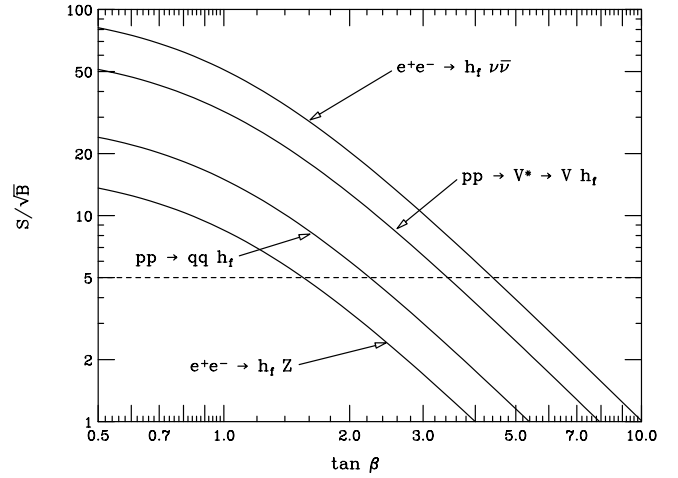

FIG. 1.   Signal/background ratio for a fermiophobic Higgs h_f decaying into two photons, as a function of $\tan\beta$. Two production mechanisms are considered at the LHC and two at a future LC ($\sqrt{s} = 500$ GeV).

$$\mathrm{B\,R}(h_f \to \gamma\gamma)/\mathrm{BR}(\phi^0 \to \gamma\gamma) \approx 10. \qquad (3)$$

In Fig. 1 we plot $S/\sqrt{B}$ for h_f as a function of $\tan\beta$. We include the production mechanisms (i)-(iv) and take $m_{h_f} = 120$ GeV. For mechanism (ii) we use the results of the simulation in [34]. Each curve is of the simple form:
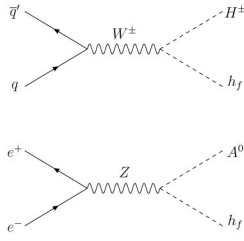
$$S/\sqrt{B} = 10K_i\cos^2\beta, \qquad (4)$$

where K_i ($i = 1, 4$) corresponds to the SM Higgs $S^\phi/\sqrt{B}$ for each of the mechanisms (i)-(iv). We assume luminosities ($\mathcal{L}$) of 50 fb^{-1} for (i), (ii) and 1000 fb^{-1} for (iii), (iv). For other choices of $\mathcal{L}$ the $S/\sqrt{B}$ scales as $\sqrt{\mathcal{L}}$. One can see that all the mechanisms offer spectacular signals ($S/\sqrt{B} >> 5$) *when* there is little suppression in the cross section at low $\tan\beta$. However, $S/\sqrt{B}$ falls rapidly as $\tan\beta$ increases, and $S/\sqrt{B} < 5$ at some critical value $\tan\beta_C$. In Fig. 1, $\tan\beta_C$ varies between two and five. Hence, unless $\tan\beta$ is fairly small, a relatively light h_f (even $m_{h_f} < <120$ GeV) may escape detection at both the LHC and LC.

B. Complementary mechanisms

Complementary mechanisms play an important role in the search for h_f in the case of the $h_f VV$ coupling being suppressed. The process $p\bar{p} \to H^\pm h_f$ [26] at the Tevatron Run II, although offering promising rates for lighter m_{h_f}, is significantly suppressed for $m_{h_f}, m_{H^\pm} > 100$ GeV. We shall consider the following direct production mechanisms of h_f,

(i) At the LHC: $pp \to H^\pm h_f, A^0 h_f$.

(ii) At a LC: $e^+e^- \to A^0 h_f$.

FIG. 2. Curves with constant branching ratios BR($H^{\pm} \to W^*h_f$) = 0.5, 0.9, and 0.99 and BR($H^{\pm} \to \tau\nu$) = 0.5, 0.65, and 0.9 in the $m_{h_f} - \tan\beta$ plane for m_{H^+} = 150 GeV.

We are not aware of explicit signal-background simulations for these channels. Mechanism (i) is expected to be ineffective for decays of Higgs bosons to fermions, but for the case of $h_f \to \gamma\gamma$ might offer more promising detection prospects. Mechanism (ii) is the LC analogy of the LEP2 process and is usually absent in discussions of the minimal supersymmetric standard model Higgs bosons due to the strong suppression of $\cos^2(\beta - \alpha)$ for $m_A \gtrsim m_Z$ in such models. However for a h_f in the region of suppressed $h_f VV$ coupling it offers promising rates. Detection prospects for $e^+e^- \to A^0 h_f$, $h_f \to \gamma\gamma$ at larger $\tan\beta$ might be comparable to those for the Higgsstrahlung channel $e^+e^- \to Zh_f$ at low $\tan\beta$ (see Fig. 1).

The cross section formulas for all the processes can be found in [37,38]. They depend on three input parameters, m_{h_f}, $\tan\beta$, and one of m_A, $m_{H^{\pm}}$. We sum over $\sigma(pp \to H^+h_f)$ and $\sigma(pp \to H^-h_f)$.

C. Decays $H^{\pm} \to h_f W^*$ and $A^0 \to h_f Z^*$

The experimental signature arising from the complementary mechanisms in Section III B depends on the decay products of $H^{\pm}$ and A^0. It has been shown [39] (see also [40]) that both BR($H^{\pm} \to h_f W^*$) and BR($A^0 \to h_f Z^*$) can be very large in the 2HDM (Model I) since the decay widths to the fermions ($H^{\pm} \to f'\bar{f}$, $A^0 \to f\bar{f}$) scale as $1/\tan^2\beta$. Thus in the region of $\tan\beta > 10$ (where the complementary mechanisms are important) the fermionic channels are very suppressed, enabling the decays $H^{\pm} \to h_f W^*$ and $A^0 \to h_f Z^*$ to become the dominant channels. Reference [39] studied the BRs for Higgs boson masses of interest at LEP2. In this paper we are extending their analysis to include masses of interest at the LHC and a LC.

In Fig. 2 we plot curves of constant charged Higgs branching ratio in the $m_{h_f} - \tan\beta$ plane for $m_{H^{\pm}}$ = 150 GeV. The solid curves correspond to BR($H^{\pm} \to W^*h_f$) and the dashed lines correspond to BR($H^{\pm} \to \tau\nu$). The decay that interests us here $H^{\pm} \to W^*h_f$ dominates at low values of m_{h_f} because in this case W^* is more on shell; it also dominates at large values of $\tan\beta$ because the competing $H^{\pm}f\bar{f}$ decays are suppressed by $1/\tan^2\beta$. In contrast, the decay $H^{\pm} \to \tau\nu$ dominates at large values
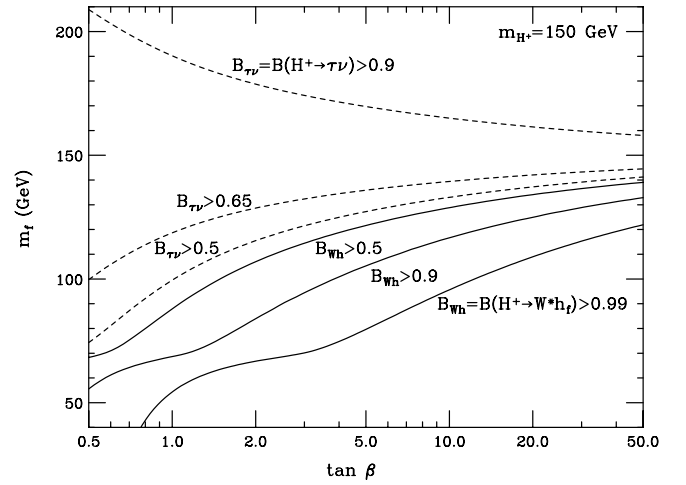
of m_{h_f} and small values of $\tan\beta$. For $m_f > 150$ GeV, the fermiophobic Higgs is no longer real.

Figure 3 is a similar plot where we have curves with constant CP-odd Higgs branching ratios in the $m_{h_f} - \tan\beta$ plane for $m_A = 150$ GeV. As in the previous figure, BR($A^0 \to Zh_f$) is in solid lines and dominates when m_{h_f} is small and $\tan\beta$ is large, and BR($A^0 \to b\bar{b}$) is in dashed lines and dominates when m_{h_f} is large and $\tan\beta$ is small. By comparing Figs. 2 and 3 it is apparent that the region of domination of the decay $A^0 \to Zh_f$ in the $m_{h_f} - \tan\beta$ plane is smaller than that for the decay $H^{\pm} \to Wh_f$. This is because the decay width for $A^0 \to b\bar{b}$ is larger than that for $H^{\pm} \to \tau\nu$, since the former $\sim m_b^2$ while the latter $\sim m_\tau^2$.

In the lower regions of $m_{h_f} - \tan\beta$ parameter space where BR($H^{\pm} \to W^*h_f$) > 0.5 and BR($A^0 \to Zh_f$) > 0.5,
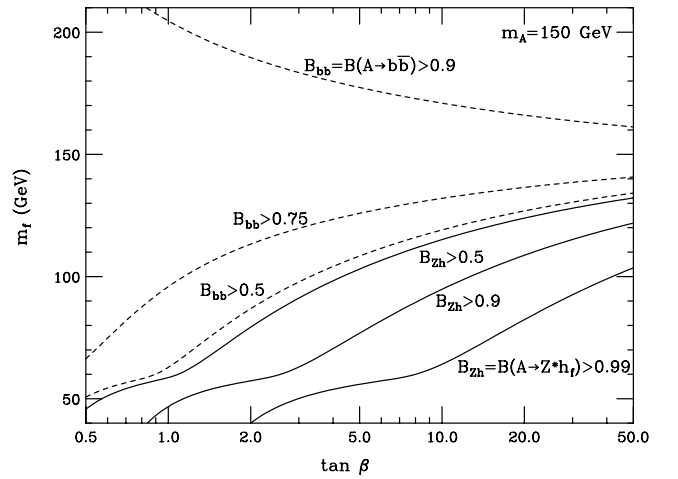
FIG. 3. Curves with constant branching ratios BR($A^0 \to Z^*h_f$) = 0.5, 0.9, and 0.99, and BR($A^0 \to b\bar{b}$) = 0.5, 0.75, and 0.9 in the $m_{h_f} - \tan\beta$ plane for m_A = 150 GeV.

a directly produced fermiophobic Higgs boson may be accompanied by one produced indirectly from the decay of $H^{\pm}$ or A^0. This scenario would give rise to double h_f production with subsequent decay of $h_f h_f \rightarrow \gamma\gamma\gamma\gamma$, $VV\gamma\gamma$ and $VVVV$. For light h_f ($m_{h_f} < 80$ GeV), the signal $\gamma\gamma\gamma\gamma$ would dominate, as discussed in [39] at LEP and in [26] for the Tevatron Run II. For $m_{h_f} \approx 95$ GeV the channels $VV\gamma\gamma$ and $VVVV$ would be comparable in number to $\gamma\gamma\gamma\gamma$, while for $m_{h_f} > 100$ GeV, the $VVVV$ would start to be the dominant signature. We stress that double h_f production requires a large BR($H^{\pm} \rightarrow h_f W^*$) or BR($A^0 \rightarrow h_f Z^*$) and is a feature of the 2HDM (Model I). The analogous BRs in other versions of the 2HDM are much smaller, although large BRs are also possible in triplet models with fermiophobia [41].

IV. PRODUCTION CROSS-SECTIONS

For the production cross sections at the LHC we shall be using the MRST2002 set from [42]. Note that QCD corrections increase the tree-level cross section by a factor of around 1.3 [38]. In our analysis we shall present results using the tree-level formulas only. In the following figures we plot contour lines of constant cross section at both the LC and LHC for different choices of parameters m_{h_f}, $\tan\beta$, $m_{H^{\pm},A^0}$. We will show results for $e^+e^- \rightarrow h_f A^0$ and $pp \rightarrow H^{\pm}h_f$. The cross section for $pp \rightarrow h_f A^0$ is half that of $pp \rightarrow H^{\pm}h_f$ for $m_A = m_{H^{\pm}}$.

In Fig. 4 we have contours of constant production cross section at the LC with $\sqrt{s} = 500$ GeV in the $\tan\beta - m_{h_f}$ plane, where m_{h_f} is the fermiophobic Higgs boson mass. The four dashed lines correspond to the standard production mechanism $e^+e^- \rightarrow Zh_f$ with its cross section being

equal to $\sigma(Zh_f) = 20, 25, 30,$ and 35 fb. The four solid lines correspond to the complementary mechanism $e^+e^- \rightarrow A^0h_f$ with the same values for its cross section $\sigma(A^0h_f)$ and taking $m_A = 150$ GeV. The Higgsstrahlung production mechanism dominates at small $\tan\beta$ since, in this model, the cross section is proportional to $\cos^2\beta$ (as explained in Section III A). On the contrary, the production of a fermiophobic Higgs in association with a CP-odd Higgs A^0 dominates at large $\tan\beta$ due to the dependence of the cross section on $\sin^2\beta$. For this reason, in the case of $\sigma(Zh_f)$ the constant cross section contours strongly depend on $\tan\beta$, and for $\tan\beta \gtrsim 2$ the cross section is already smaller than 20 fb. Equally sharp but opposite dependence on $\tan\beta$ is observed for the constant $\sigma(A^0h_f)$ contours. This effect is evident as a clear depression of the observability of h_f at around $\tan\beta = 1 - 2$, where both cross sections are smaller than 20 fb for $m_{h_f} \gtrsim 130$ GeV.

In Fig. 5 we have similar contours of constant production cross section, but this time at the LHC with $\sqrt{s} = 14$ TeV in the $\tan\beta - m_{h_f}$ plane. The four dashed lines correspond to the standard mechanism $pp \rightarrow Wh_f$ with values $\sigma(Wh_f) = 70, 100, 130,$ and 160 fb. The four solid lines correspond to the complementary mechanism $pp \rightarrow H^{\pm}h_f$ for the same values of the cross section $\sigma(H^{\pm}h_f)$ and taking $m_{H^{\pm}} = 150$ GeV. As before, the standard mechanism is dominant at low values of $\tan\beta$ and the complementary mechanism dominates at high $\tan\beta$. This is due to a dependence of the partonic cross section on $\cos^2\beta$ and $\sin^2\beta$ respectively. Because of phase space effects, the dependence on m_{h_f} is stronger compared with the LC case making the equal cross section contours less vertical. For this reason, the depression already observed in the previous figure is less pronounced at the LHC.
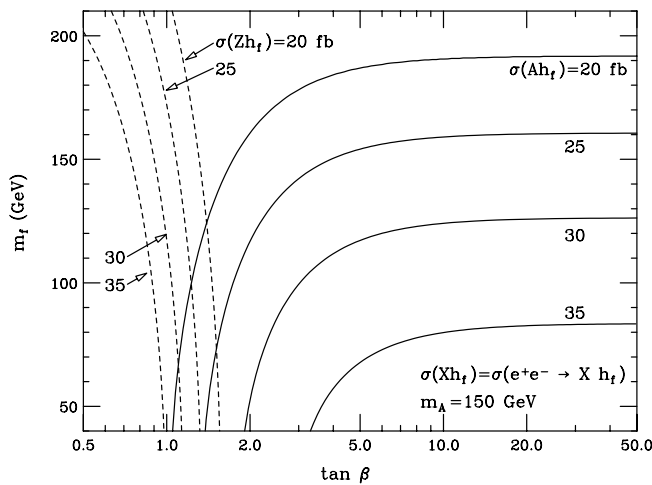

FIG. 4. Curves with constant production cross section $\sigma = 20, 25, 30,$ and 35 fb at a future LC in the $m_{h_f} - \tan\beta$ plane for $m_A = 150$ GeV.
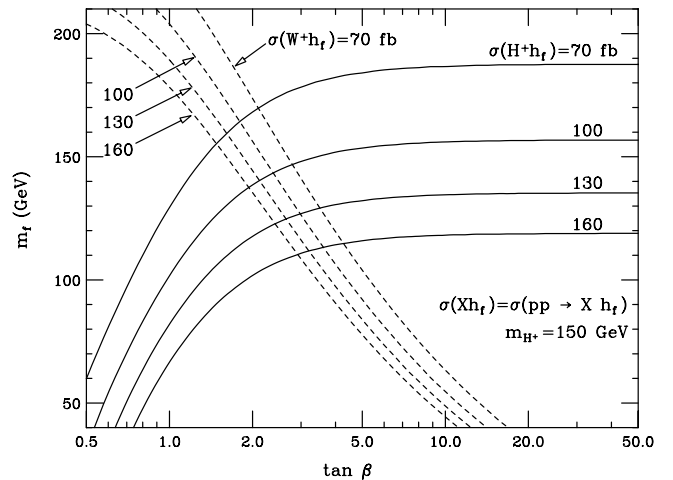
FIG. 5. Curves with constant production cross section $\sigma = 70\ 100\ 130,$ and 160 fb at the LHC in the $m_{h_f} - \tan\beta$ plane for $m_{H^+} = 150$ GeV.

In Fig. 6 and 7 we plot contours of constant production cross section at the LC and LHC, respectively, in the $m_A - m_{h_f}$ plane for the LC and in the $m_{H^+} - m_{h_f}$ plane for the LHC using the same numerical values for the cross sections as in Figs. 4 and 5. In both cases we take $\tan\beta = 20$, where the standard production mechanisms are very suppressed. If a realistic simulation of the signal were made and the minimum number of events $N_{\min}$ were known for the signal to be observable, the observable cross sections would be of the type $\sigma > N_{\min}/\mathcal{L}$ implying that the region below and to the left of the curves in both figures would be observable. From the figures we see that to increase the region of observability, the minimum cross section needs to be decreased more sharply at the LHC rather than at the LC.

In a similar way, in Figs. 8 and 9 we plot contours of constant production cross section at the LC and LHC, respectively, in the $m_A - \tan\beta$ plane for the LC and in the $m_{H^+} - \tan\beta$ plane for the LHC. The chosen values for the cross sections are the same as in the previous figures, and we take a fermiophobic Higgs mass $m_{h_f} = 120$ GeV in both cases. The largest cross sections lie towards the bottom right-hand corner of the figure. The stronger dependence of $\sigma(pp \to H^\pm h_f)$ on m_{H^+} is evident from the figures when compared with the dependence of $\sigma(e^+e^- \to A^0 h_f)$ on m_A.

In all the situations studied here, the directly produced fermiophobic Higgs boson decays into two photons with a branching ratio close to unity if $m_{h_f} \lesssim 80$ GeV, close to 0.5 for $m_{h_f} \sim 95$ GeV and near 0.01 for $m_{h_f} \sim 145$ GeV. In the case of complementary production at the LHC and LC shown in the previous graphs, the number of four photon events will be maximized for larger BR$(A^0 \to Zh_f)$ and BR$(H^\pm \to W^* h_f)$ and lower m_{h_f}. Comparing

Figs. 3 and 4 we can see that (for $m_A = 150$ GeV) if the model lies below the curve $\sigma(e^+e^- \to A^0 h_f) \approx 30$ fb in the $m_{h_f} - \tan\beta$ plane then the majority of events will be of the four photon type at the LC. Similarly, comparing Figs. 2 and 5 we see that (for $m_{H^+} = 150$ GeV) if the model lies below the curve $\sigma(pp \to H^\pm h_f) \approx 130$ fb in the $m_{h_f} - \tan\beta$ plane, then a four photon signal would be plentiful at the LHC. Identifying a lepton from the decay of W^* or Z^* would further reduce backgrounds. After applying a realistic photon identification efficiency for four photons ($0.8^4 \approx 0.4$) [34] and multiplying by the appropriate BR factors, signal sizes for $\gamma\gamma\gamma\gamma + l^\pm$ in excess of a few fb are possible in a sizeable region of the $m_{h_f} - \tan\beta$ plane.

At the LHC, the main backgrounds for the $\gamma\gamma\gamma\gamma + l^\pm$ are expected to be the irreducible $\gamma\gamma\gamma\gamma + l^\pm$ from genuine photon production, and the reducible four jet plus $l^\pm$, where all four jets are misidentified as a photon. MadEvent [43] estimates the irreducible background to be $\sim 10^{-6}$ fb and thus entirely negligible. The four jet plus $l^\pm$ was estimated to be $\sim 130\,000$ fb, but this fake photon background can be reduced to a negligible size after applying realistic rejection factors of 10^3 for each jet [34]. Hence, we conclude that $\gamma\gamma\gamma\gamma + l^\pm$ is a robust, relatively background free signature at the LHC. A detailed study of detection prospects in all the channels $\gamma\gamma\gamma\gamma$, $\gamma\gamma VV$, and $VVVV$ will be considered in a separate work.

V. CONCLUSIONS

We have considered the phenomenology of a fermiophobic Higgs boson (h_f) at the Large Hadron Collider and an e^+e^- linear collider. We showed that the production mechanisms $pp \to H^\pm h_f, A^0 h_f$, and $e^+e^- \to A^0 h_f$ offer
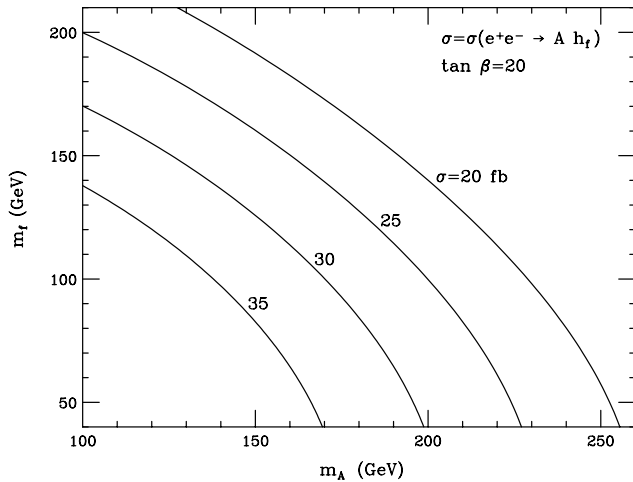
FIG. 6. Curves with constant production cross section $\sigma = 20, 25, 30$, and 35 fb at a future LC in the $m_{h_f} - m_A$ plane for $\tan\beta = 20$.
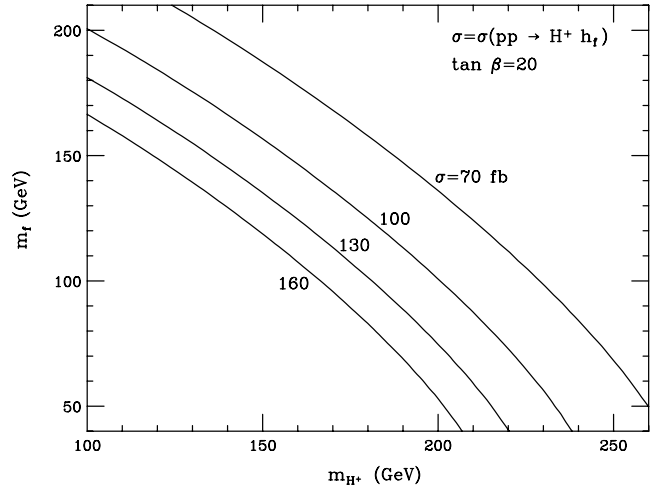
FIG. 7. Curves with constant production cross section $\sigma = 70, 100, 130$, and 160 fb at the LHC in the $m_{h_f} - m_{H^+}$ plane for $\tan\beta = 20$.
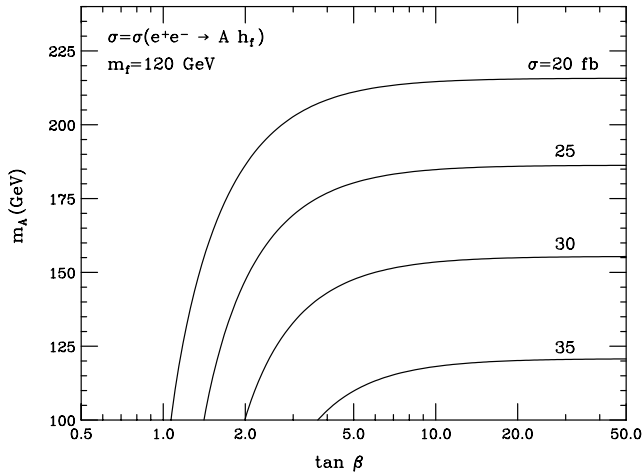
FIG. 8. Curves with constant production cross section $\sigma = 20, 25, 30,$ and 35 fb at a future LC in the $m_A - \tan\beta$ plane for $m_{h_f} = 120$ GeV.

FIG. 9. Curves with constant production cross section $\sigma = 70, 100, 130,$ and 160 fb at the LHC in the $m_{h_f} = 120$ GeV.

promising cross sections in the region where the conventional mechanisms $pp \to W^{\pm}h_f$ and $e^+e^- \to h_fZ$ are very suppressed. A more complete search strategy at both these colliders would include these complementary production mechanisms. The potentially large branching ratios for $H^{\pm} \to h_fW^*$ and $A^0 \to h_fZ^*$ would lead to double h_f production, with subsequent signatures $\gamma\gamma\gamma\gamma$, $\gamma\gamma VV$ and $VVVV$, which need experimental simulations. Production cross sections are similar at both 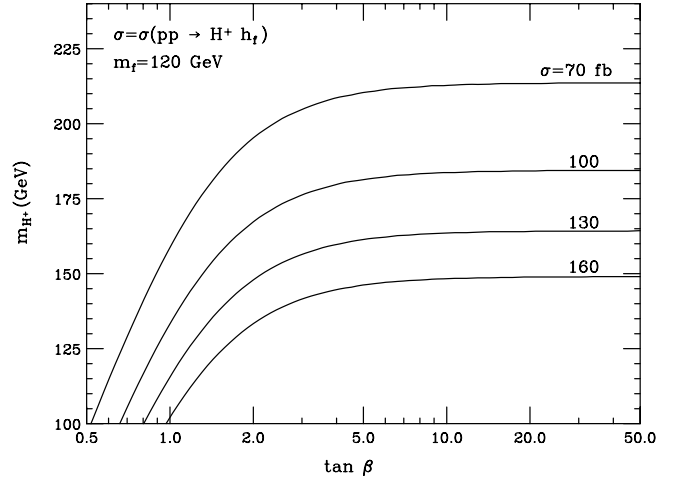machines, but the larger luminosity and smaller backgrounds at the LC would permit precision measurements necessary to determine the exact nature of the observed fermiophobic Higgs boson.

ACKNOWLEDGMENTS

[1] J. F. Gunion, H. E. Haber, G. L. Kane, and S. Dawson, *The Higgs Hunter's Guide*, (Addison-Wesley, Reading, MA, 1989).

[2] S. L. Glashow and S. Weinberg, Phys. Rev. D **15**, 1958 (1977).

[3] V. D. Barger, J. L. Hewett, and R. J. Phillips, Phys. Rev. D **41**, 3421 (1990).

[4] ALEPH Collaboration, R. Barate *et al.*, Phys. Lett. B **565**, 61 (2003).

[5] OPAL Collaboration, G. Abbiendi *et al.*, Eur. Phys. J. C **18**, 425 (2001); ALEPH Collaboration, A. Heister *et al.*, Phys. Lett. B **544**, 25 (2002).

[6] A. G. Akeroyd, Phys. Lett. B **377**, 95 (1996);

[7] T. J. Weiler, in *Proceedings of the 8th Vanderbilt Int. Conf. on High Energy Physics, Nashville, TN, 1987*, edited by J. Brau and R. Panvini (World Scientific, Singapore, 1988), p. 219.

[8] H. E. Haber, G. L. Kane, and T. Sterling, Nucl. Phys. B **161**, 493 (1979).

[9] H. Georgi and M. Machacek, Nucl. Phys. B **262**, 463 (1985); M. S. Chanowitz and M. Golden, Phys. Lett. B **165**, 105 (1985); J. F. Gunion, R. Vega, and J. Wudka, Phys. Rev. D **42**, 1673 (1990).

[10] V. D. Barger, N. G. Deshpande, J. L. Hewett, and T. G. Rizzo, hep-ph/9211234.

[11] H. Pois, T. J. Weiler, and T. C. Yuan, Phys. Rev. D **47**, 3886 (1993).

[12] A. Stange, W. J. Marciano, and S. Willenbrock, Phys. Rev. D **49**, 1354 (1994).

[13] M. A. Díaz and T. J. Weiler, hep-ph/9401259.

[14] A. G. Akeroyd, Phys. Lett. B **368**, 89 (1996).

[15] A. Barroso, L. Brucher, and R. Santos, Phys. Rev. D **60**, 035005 (1999).

[16] L. Brucher and R. Santos, Eur. Phys. J. C **12**, 87 (2000).

[17] OPAL Collaboration, G. Abbiendi *et al.*, Phys. Lett. B **544**, 44 (2002).

[18] DELPHI Collaboration, P. Abreu *et al.* Phys. Lett. B **507**, 89 (2001); Eur. Phys. J. C **35**, 313 (2004).

[19] ALEPH Collaboration, A. Heister *et al.* Phys. Lett. B **544**, 16 (2002).

[20] L3 Collaboration, P. Achard *et al.* Phys. Lett. B **534**, 28 (2002); Phys. Lett. B **568**, 191 (2003).

[21] L3 Collaboration, P. Achard *et al.* hep-ex/0307010.

[22] D0 Collaboration, B. Abbott *et al.* Phys. Rev. Lett. **82**, 2244 (1999).

[23] CDF Collaboration, T. Affolder *et al.* Phys. Rev. D **64**, 092002 (2001).

[24] S. Mrenna and J. Wells, Phys. Rev. D **63**, 015006 (2001).

[25] G. Landsberg and K. T. Matchev, Phys. Rev. D **62**, 035004 (2000).

[26] A. G. Akeroyd and M. A. Díaz, Phys. Rev. D **67**, 095007 (2003).

[27] A. Arhrib, M. Capdequi Peyranere, W. Hollik, and S. Penaranda, Phys. Lett. B **579**, 361 (2004).

[28] A. G. Akeroyd, J. Phys. G **24**, 1983 (1998).

[29] X. Calmet and H. Fritzsch, Phys. Lett. B **496**, 190 (2000).

[30] I. F. Ginzburg, M. Krawczyk, and P. Osland, Nucl. Instrum. Methods Phys. Res., Sect. A **472**, 149 (2001).

[31] A. Djouadi, W. Kilian, M. Muhlleitner, and P. M. Zerwas, Eur. Phys. J. C **10**, 45 (1999); S. Kanemura and C. P. Yuan, Phys. Lett. B **530**, 188 (2002); Q. H. Cao, S. Kanemura, and C. P. Yuan, Phys. Rev. D **69**, 075008 (2004).

[32] CMS Collaboration, M. Dubinin, V. Ilyin, and V. Savrin, Note 1997/101 (1997).

[33] D. Rainwater and D. Zeppenfeld, J. High Energy Phys. **9712**, 005 (1997).

[34] K. Cranmer, B. Mellado, W. Quayle, and S. L. Wu, hep-ph/0401088.

[35] E. Boos, J. C. Brient, D. W. Reid, H. J. Schreiber, and R. Shanidze, Eur. Phys. J. C **19**, 455 (2001).

[36] A. Dedes, S. Heinemeyer, S. Su, and G. Weiglein, Nucl. Phys. B **674**, 271 (2003).

[37] E. Eichten, I. Hinchliffe, K. D. Lane, and C. Quigg, Rev. Mod. Phys. **56**, 579 (1984); **58**, 1065 (1986).

[38] S. Dawson, S. Dittmaier, and M. Spira, Phys. Rev. D **58**, 115012 (1998).

[39] A. G. Akeroyd, Nucl. Phys. **B544**, 557 (1999).

[40] F. M. Borzumati and A. Djouadi, Phys. Lett. B **549**, 170 (2002).

[41] A. G. Akeroyd, Phys. Lett. B **442**, 335 (1998).

[42] A. D. Martin, R. G. Roberts, W. J. Stirling, and R. S. Thorne, Eur. Phys. J. C **23**, 73 (2002).

[43] F. Maltoni and T. Stelzer, J. High Energy Phys. 0302 (2003) 027.